PHYSICAL REVIEW B VOLUME 4, NUMBER 6 15 SEPTEMBER 1971

Mobility Anisotropy of Electrons in Inversion Layers on Oxidized Silicon Surfaces

Tai Satô, Yoshiyuki Takeishi, and Hisashi Hara
Toshiba Research and Development Center, Tokyo Shibaura Electric Company, Ltd., Komukai, Kawasaki, Japan

and

Yoshihiko Okamoto
I. C. Engineering Department, Tokyo Shibaura Electric Company, Ltd., Komukai, Kawasaki, Japan

(Received 10 December 1970)

Measurements of the field-effect mobility of electrons in n-type inversion layers of Si as functions of the crystalline orientation of the surface and of the azimuthal direction of the current path within the layers are reported. Significant mobility anisotropy observed over a range of strong electric fields perpendicular to the surface at temperatures from 77 to 320 °K contrasts substantially with that in the case of p-type inversion layers reported previously. The anisotropy at room temperature can be successfully interpreted in terms of the effective-mass anisotropy calculated on the basis of Stern and Howard's formula for the two-dimensional carriers. For a full understanding of the experimental results, particularly at low temperatures, theoretical investigations including the anisotropy of the relaxation time are required, but have not been explored enough. Extensive data on the dependences of the mobility on the electric field and temperature as well as bulk-acceptor concentration are presented and discussed in the light of existing scattering theories. Some hole-mobility data are included for comparison.

I. INTRODUCTION

In a previous paper[1] on physical properties of p-type inversion layers on oxidized silicon surfaces in the structure of the metal-oxide-semiconductor field-effect transistor (MOSFET), pronounced effects of the crystalline orientation of the surface and the direction of current flow on the field-effect mobility of holes were reported. Ten surface orientations lying in the $\langle 100\rangle$ and $\langle 01\bar{1}\rangle$ zones and two specified directions of the flow on each plane, except (111) and (100), were used. It was concluded that the mobility anisotropy at room temperature under strong electric fields applied perpendicularly to the surface is mainly due to the anisotropy of the effective mass of heavy holes whose motion in the direction of the surface normal is quantized. The effective masses were calculated by Maeda[2] on the basis of a $\langle 110\rangle$-swelling energy contour[3] that is pertinent to the high-energy heavy holes. Possible anisotropy of the carrier mean free time was fully neglected. An over-all result of this study is summarized in the lower half of Fig. 2 in the present paper. This type of mobility anisotropy was first observed and theoretically investigated for some typical surface orientations by Colman, Bate, and Mize,[4] who utilized the band-edge structure, which is not a good approximation for the high-energy heavy holes.

In view of this result one can naturally expect that the mobility anisotropy in the case of electron motion in n-type inversion layers should appear quite differently, since the conduction-band structure is very different from the valence-band structure. Stern and Howard[5] have calculated, with a theory in the effective-mass-approximation framework, the effective masses of the electrons moving like a two-dimensional electron gas on the (100), (111), and (011) planes when their motion perpendicular to the surface is quantized. If the effective mass again features the mobility μ of the electron, mobility anisotropy should appear such that $\mu(100)$ is highest and $\mu(011)\perp\langle 01\bar{1}\rangle$ is higher than $\mu(011)\parallel\langle 01\bar{1}\rangle$. Notations $(hkl)\perp$ and $\parallel\langle h'k'l'\rangle$ mean the directions of the current paths perpendicular to and parallel to $\langle h'k'l'\rangle$ on the (hkl) plane, respectively, throughout this paper. Experimental evidence showing that $\mu(100)$ is higher than $\mu(111)$ in MOSFET's under a strong electric field is shown in papers by, for example, Fang and Fowler[6] and Murphy, Berz, and Flinn.[7] Ohwada, Maeda, and Tanaka[8] reported that we have $\mu(100) > \mu(311) > \mu(211) > \mu(111) \approx \mu(011)$ in accordance with the order of calculated reciprocal effective masses of electrons.

The primary purpose of the present study is to investigate how the effective-mass anisotropy appears in the anisotropy of the field-effect mobility of the electrons in the inversion layers at temperatures between 320 and 77 °K, by the use of the same orientations and directions as those used in the hole-mobility study.[1] In Sec. II the corresponding effective masses are calculated on the basis of Stern and Howard's formula. Experimental procedures are described in Sec. III. In Sec. IV observed mobility anisotropy at room temperature is success-

fully compared with the effective-mass anisotropy including the effect of carrier population in energy levels above the lowest subband. Mobility anisotropy at low temperatures points to an anisotropy of the relaxation time. Data on the dependences of the mobility on the electric field and temperature as well as on bulk-acceptor concentration and some of the data on the hole mobility are presented for comparison in Sec. V. The data which manifest themselves in the complexity of the phenomena are discussed by existing theories of carrier scattering mechanisms. It is emphasized that although Fang and Fowler[6] reported extensive data on the Hall mobility, conductivity mobility, and field-effect mobility on (100), (111), and (011) over a wide range of temperatures down to 4.2 °K, the present data will provide new information because more orientations are used and the direction of current path is specified. Concluding remarks on the problem remaining unsolved are described in Sec. VII.

II. CALCULATION OF ANISOTROPIC EFFECTIVE MASSES OF ELECTRONS

It is known that, when a strong electric field is applied to the semiconductor surface in the direction normal to the surface, carrier motion in this direction is quantized.[9] When the inverted surface channel is approximated by a triangular potential in direction z, quantized energy levels E_{zn} for a nondegenerate constant-energy surface are given by[4]

$$E_{zn}=[eF_z\hbar/(2m_z)^{1/2}]^{2/3}\gamma_n\ , \qquad n=0,\ 1,\ 2,\ \ldots. \tag{1}$$

Here γ_n is the $(n+1)$th zero of the Airy function, F_z is the normal electric field at the surface, and m_z is the effective mass of carriers in the z direction. When this quantization occurs, the carrier behaves as a two-dimensional electron gas in the xy plane parallel to the surface. In this case, when anisotropy of the relaxation τ is neglected, the carrier mobility μ_{ij} is expressed as

$$\mu_{ij}=e\tau(m^{-1})_{ij}, \qquad i,\ j=1,\ 2 \tag{2}$$

where $(m^{-1})_{ij}$ is the ij element of the reciprocal-effective-mass tensor of the second rank.

Calculation of $(m^{-1})_{ij}$ by the effective-mass theory is easier for electrons than for holes, because of nondegeneracy at the conduction-band edges, which is in contrast to the threefold degeneracy of the valence-band edge. For the conduction bands with multiple minima of silicon Stern and Howard[5] calculated the principal effective masses for surface orientations of (100), (011), and (111) in terms of m_t and m_l, which are, respectively, the transverse and longitudinal effective masses in the bulk at the conduction-band edges.

Making use of Stern and Howard's general formulas [see Eq. (13) in Ref. 5], we extend the calculation of the reciprocal effective masses to the cases of electrons moving on the planes lying in a $\langle 100\rangle$ zone and on the planes lying in a $\langle 01\bar{1}\rangle$ zone. We define the x and y directions to be the directions parallel and perpendicular to the $\langle 100\rangle$ direction on the planes in the $\langle 100\rangle$ zone, respectively, and to be the directions parallel and perpendicular to the $\langle 01\bar{1}\rangle$ direction in the planes in the $\langle 01\bar{1}\rangle$ zone, respectively. We need only a transformation of the original coordinates ξ, η, and ζ passing through the principal axes of the constant-energy ellipsoids (Fig. 1) to those for the specified surface orientations. For convenience, the six band edges are arbitrarily numbered as indicated in Fig. 1(a).

For the $\langle 100\rangle$ zone the coordinates of concerned orientations, $\xi'=\xi$, η', and ζ', are specified with angle θ around the ξ axis, as shown in Fig. 1(a). Results of the calculations of the reciprocal effective masses $m_x^{-1}\parallel\langle 100\rangle$, $m_y^{-1}\perp\langle 100\rangle$, and m_z^{-1} for each band edge are given in Table I(a). For the $\langle 01\bar{1}\rangle$ zone, the necessary transformation is as follows: First, rotate the η and ζ axes around ξ by 45°, and next, rotate the new η' and the $\xi'=\xi$ axes around the new ζ' axis by θ. These procedures are illustrated in Fig. 1(b). The transformed coordinates are ξ'', η'', and ζ''. When $\theta=0$, the plane perpendicular to the η'' axis is (011), and when $\cos^2\theta=\frac{1}{3}$, it is (111). It should be noted that for ellipsoids 1–4 the reciprocal masses $(m^{-1})_{11}$ and $(m^{-1})_{22}$ are not principal values of the constant-energy ellipses associated with motion in the surface, but the equivalent-energy ellipsoids 1 and 3, and 2 and 4 cancel out the off-diagonal elements, and thus we shall tabulate only the reciprocal-effective-mass tensor elements $(m^{-1})_{11}$ and $(m^{-1})_{22}$. Hereafter we call these elements m_x^{-1} and m_y^{-1}, respectively. Hence, in this case, the product $m_xm_ym_z$ is not equal to the product $m_x'm_y'm_z'$ of the principal effective masses in the bulk. The results thus calculated for $m_x^{-1}\parallel\langle 01\bar{1}\rangle$, $m_y^{-1}\perp\langle 01\bar{1}\rangle$, and m_z^{-1} are summarized in Table I(b). For the surface orientations involved in the present experimental study the numerical values of the reciprocal effective masses in units of the reciprocal free-electron mass m_e^{-1} are given in Table II.

III. MEASUREMENTS

Experimental n-channel transistors used in this experiment have a rectangular channel path 200 μm long (L) and 600 μm wide (W). Ten surface orientations and two specified source-to-drain directions on them (refer to Table II and Fig. 2) on p-type ~8–25-Ω cm silicon material are selected. These features are the same as those of the p-channel

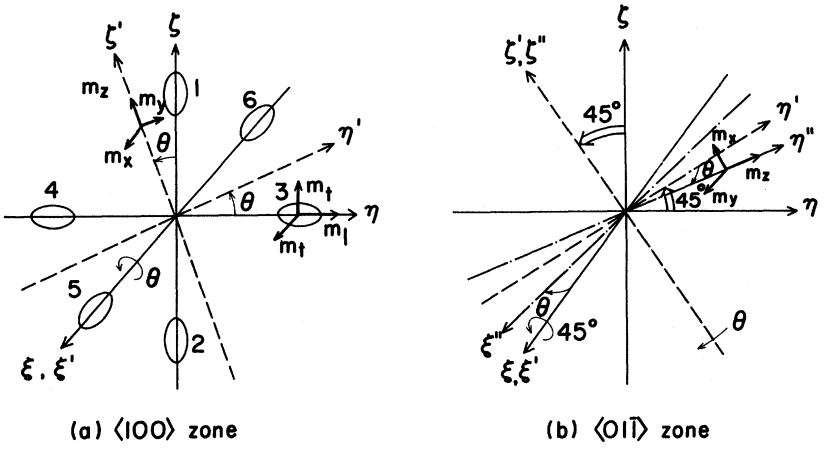

FIG. 1. Illustrations of surface orientations with respect to crystalline orientation. In ⟨100⟩ zone (a), the surface normal is a ξ' axis and θ is the angle between the ξ and ξ' axes. In ⟨01$\bar{1}$⟩ zone (b), the surface normal is an η'' axis and θ is the angle between the η' and η'' axes.

transistors in the authors' previous study.[1] The source and drain islands were doped with phosphorus. A p^+ guard ring is further provided around the active transistor region so as to prevent possible current leakage. The gate oxide grown in steam at 1145 °C is about 2000 Å thick, and doped with phosphorus for stabilization. Before and after the gate electrode of aluminum was provided, the specimens were heat treated in a hydrogen atmosphere at 500 °C for 15 min and at 50 °C for 15 min, respectively, to decrease the density of surface states.

The field-effect mobility μ_{FE} is determined by measurement of the transconductance g_m under the triode operation of the transistor:

$$\mu_{FE} = g_m L^2 / C_{ox} V_D , \tag{3}$$

where C_{ox} is the gate-oxide capacitance and V_D the source-drain voltage. The transconductance $|\partial I_D / \partial V_G|_{V_D}$ was measured directly using an ac modulation technique similar in principle to that described by Fang and Fowler.[6] The drain voltage is fixed at 50 mV and the gate signal is 1 kHz, 200 mV rms. The field-effect mobility defined by Eq. (3) is accurate, except when the gate voltage V_G is close to the threshold voltage V_T of the transistor within 0.5 V. Equation (3) assumes no trapping of induced carriers into surface states at the interface. Since the present samples were properly annealed, and the values of μ_{FE} determined on the basis of Eq. (3) at 1 kHZ are the same as those of μ_{FE} determined by a dc method, the trapping of the induced carriers into surface states which would respond to the frequency up to 1 kHz can be neglected, although Sakaki, Hoh, and Sugano[11] reported about 10% trapping of induced carriers over a range of carrier concentration up to $3\times10^{12}/\text{cm}^2$. The threshold voltage reflecting the density of surface states ranges from −1.3 to −4.0 V at room temperature. The smaller V_T's appear on the surfaces around (100) and the larger ones appear around (111), which is the same as for the p-channel transistors.[1] The standard deviation of transconductance data among ten samples is about 1%, but the values of the oxide capacitance are scattered a little from sample to sample in a range of ±4%.

More recently dependence of the field-effect mo-

TABLE I. Reciprocal effective masses of electrons in the three specified directions on the planes lying in the ⟨100⟩ and ⟨01$\bar{1}$⟩ zones for the six band edges. The principal masses at the conduction-band edges of the bulk are m_t, m_t, and m_l. Angle θ specifies the surface orientation (see Fig. 1).

(a) ⟨100⟩ zone

Band edge	Valley	$m_x^{-1} \parallel \langle 100\rangle$	$m_y^{-1} \perp \langle 100\rangle$	m_z^{-1}
5, 6	(100)	m_l^{-1}	m_t^{-1}	m_t^{-1}
1, 2	(001)	m_t^{-1}	$(m_t\cos^2\theta + m_l\sin^2\theta)^{-1}$	$\cos^2\theta\, m_l^{-1} + \sin^2\theta m_t^{-1}$
3, 4	(010)	m_t^{-1}	$(m_l\cos^2\theta + m_t\sin^2\theta)^{-1}$	$\cos^2\theta\, m_t^{-1} + \sin^2\theta\, m_l^{-1}$

(b) ⟨01$\bar{1}$⟩ zone

Band edge	Valley	$m_x^{-1} \parallel \langle 01\bar{1}\rangle$	$m_y^{-1} \perp \langle 01\bar{1}\rangle$	m_z^{-1}
1, 2	(001)	$\dfrac{m_t^{-1}m_l^{-1}\cos^2\theta + \frac{1}{2}\sin^2\theta\,(m_t^{-1}+m_l^{-1})m_t^{-1}}{m_z^{-1}}$	$\dfrac{\frac{1}{2}(m_l^{-1}+m_t^{-1})m_t^{-1}}{m_z^{-1}}$	$\dfrac{\cos^2\theta}{2}(m_l^{-1}+m_t^{-1}) + \sin^2\theta\, m_t^{-1}$
3, 4	(010)			
5, 6	(100)	m_t^{-1}	$(m_l\cos^2\theta + m_t\sin^2\theta)^{-1}$	$\cos^2\theta\, m_t^{-1} + \sin^2\theta\, m_l^{-1}$

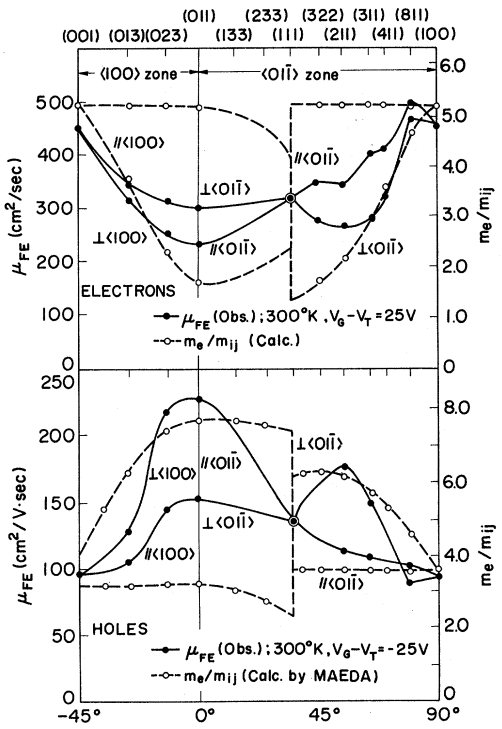

FIG. 2. Plots of the field-effect mobility of electrons (upper half) as functions of surface orientation and current-flow direction. The calculated reciprocal effective mass of electrons in the lowest subband (see Table II) is also plotted by dotted lines. Corresponding results (Ref. 1) of hole mobility are reproduced for comparison (lower half). The apparent discontinuity of the masses at the (111) [and p channel (100)] surfaces comes from the fact that only the lowest subband is considered. Near the (111) surface, the energy of upper subbands comes closer and closer to the energy of the lowest subband. If the population into these upper subbands is taken into account statistically, these discontinuities should disappear (see Table III). The resistivities of substrate and threshold voltage, respectively, for each orientation are 23.7 Ω cm, −1.4 V, (100); 24.0 Ω cm, −1.9 V, (811) ∥ ⟨01$\bar{1}$⟩; 24.6 Ω cm, −3.2 V, (811) ⊥ ⟨01$\bar{1}$⟩; 8.3 Ω cm, −1.7 V, (411) ∥ ⟨01$\bar{1}$⟩; 8.0 Ω cm, −1.6 V, (411) ⊥ ⟨01$\bar{1}$⟩; 23.1 Ω cm, −3.0 V, (311) ∥ ⟨01$\bar{1}$⟩; 24.7 Ω cm, −2.9 V, (311) ⊥ ⟨01$\bar{1}$⟩; 24.3 Ω cm, −2.3 V, (211) ∥ ⟨01$\bar{1}$⟩; 24.0 Ω cm, −2.6 V, (211) ⊥ ⟨01$\bar{1}$⟩; 8.7 Ω cm, −2.1 V, (322) ∥ ⟨01$\bar{1}$⟩; 8.5 Ω cm, −1.7 V, (322) ⊥ (01$\bar{1}$); 8.3 Ω cm, −4.0 V, (111); 27.5 Ω cm, −2.5 V, (011) ⊥ ⟨01$\bar{1}$⟩; 27.3 Ω cm, −2.2 V, (011) ∥ ⟨01$\bar{1}$⟩; 15.8 Ω cm, −2.3 V, (023) ∥ ⟨100⟩; 15.7 Ω cm, −2.5 V, (023) ⊥ ⟨100⟩; 8.7 Ω cm, −1.3 V, (013) ∥ ⟨100⟩; 8.5 Ω cm, −1.6 V, (013) ⊥ ⟨100⟩.

bility on the acceptor concentration of the substrate with (100) orientation in the range 1×10^{14} to 1×10^{17}/cm^3 was studied in an independent experiment, and the result is included in this paper.

The field-effect mobility cannot be directly compared with the conductivity mobility μ that is theoretically investigated in this paper. When the trapping effect is neglected, we have

TABLE II. Values of the reciprocal effective masses in unit of m_e^{-1} in the three directions on the planes lying in the ⟨100⟩ and ⟨01$\bar{1}$⟩ zones, given in Table I. Band-edge masses $m_t = 0.19m_e$ and $m_l = 0.98m_e$, are used (Ref. 10). Note that in the ⟨01$\bar{1}$⟩ zone, m_x^{-1} and m_y^{-1} for 1, 2, 3, and 4 band edges are not the principal values, except for the (011) plane (see text).

(a) ⟨100⟩ zone

Surface	Band edge	$m_x^{-1} \parallel \langle 100\rangle$	$m_y^{-1} \perp \langle 100\rangle$	m_z^{-1}
(001)	1, 2	5.26	5.26	1.02
	3, 4	5.26	1.02	5.26
	5, 6	1.02	5.26	5.26
		3.14	3.14	
(013)	1, 2	5.26	3.72	1.44
	3, 4	5.26	1.11	4.84
	5, 6	1.02	5.26	5.26
(012)	1, 2	5.26	2.87	1.87
	3, 4	5.26	1.22	4.41
	5, 6	1.02	5.26	5.26
(023)	1, 2	5.26	2.31	2.33
	3, 4	5.26	1.36	3.95
	5, 6	1.02	5.26	5.26
(011)	1, 2	5.26	1.71	3.14
	3, 4	5.26	1.71	3.14
	5, 6	1.02	5.26	5.26

(b) ⟨01$\bar{1}$⟩ zone

Surface	Band edge	$m_x^{-1} \parallel \langle 01\bar{1}\rangle$	$m_y^{-1} \perp \langle 01\bar{1}\rangle$	m_z^{-1}
(011)	1, 2	1.71	5.26	3.14
	3, 4	1.71	5.26	3.14
	5, 6	5.26	1.02	5.26
(233)	1, 2	2.10	4.69	3.53
	3, 4	2.10	4.69	3.53
	5, 6	5.26	1.20	4.49
(111)	1, 2	2.36	4.30	3.85
	3, 4	2.36	4.30	3.85
	5, 6	5.26	1.39	3.85
		3.33	3.33	
(322)	5, 6	5.26	1.78	3.02
	1, 2	2.64	3.88	4.26
	3, 4	2.64	3.88	4.26
(211)	5, 6	5.26	2.21	2.43
	1, 2	2.81	3.63	4.55
	3, 4	2.81	3.63	4.55
(311)	5, 6	5.26	3.00	1.79
	1, 2	2.97	3.39	4.88
	3, 4	2.97	3.39	4.88
(411)	5, 6	5.26	3.60	1.49
	1, 2	3.04	3.29	5.03
	3, 4	3.04	3.29	5.03
(811)	5, 6	5.26	4.67	1.15
	1, 2	3.11	3.18	5.20
	3, 4	3.11	3.18	5.20
(100)	5, 6	5.26	5.26	1.02
	1, 2	3.14	3.14	5.26
	3, 4	3.14	3.14	5.26

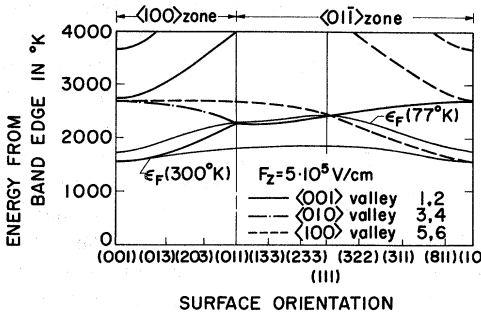

FIG. 3. Energy diagram calculated using a triangular potential approximation at $F_z = 5\times10^5$ V/cm. Fermi levels at 300 and 77 °K are shown by fine solid lines.

$$g_m = \frac{\partial I_D}{\partial V_G} = \frac{L}{W} V_D \frac{\partial \sigma}{\partial V_G}$$
$$= \frac{L}{W} e V_D \left(\frac{\partial N}{\partial V_G}\mu + \frac{\partial \mu}{\partial V_G} N \right)$$
$$\cong \frac{L}{W} V_D C_{ox} \left(\mu + (V_G - V_T)\frac{\partial \mu}{\partial V_G} \right),$$

where σ is the channel conductance and N the induced carrier concentration. Then we have

$$\mu_{FE}(V_G) \cong \mu(V_G) + (V_G - V_T)\frac{\partial \mu}{\partial V_G} \tag{4}$$

or

$$\mu(V_G) \cong \frac{1}{V_G - V_T}\int_{V_T}^{V_G} \mu_{FE}(V_G) dV_G \,. \tag{5}$$

Thus, when the mobility varies strongly with the gate field, the field-effect mobility departs appreciably from conductivity mobility. When the gate-field dependence of μ_{FE} can be approximated by

$$\mu_{FE} = \alpha (V_G - V_T)^{-\beta}, \tag{6}$$

in which α and β are constant, then

$$\mu = [\alpha/(1-\beta)](V_G - V_T)^{-\beta} \,. \tag{7}$$

In this case the field dependences of both mobilities are the same. Note that $\mu \gtrless \mu_{FE}$ when $\beta \gtrless 0$, and that $\mu_{FE} < 0$ when $\beta > 1$.

IV. MOBILITY ANISOTROPY

In the upper half of Fig. 2 the field-effect mobility μ_{FE} at $V_G - V_T = 25$V ($F_z = 4\times10^5$ V/cm) and at $T = 298$ °K, and the calculated reciprocal effective mass m_{ij}^{-1} in the lowest energy subband (see Table II) are plotted as functions of surface orientation and current path direction. The scales of μ_{FE} and m_{ij}^{-1} are normalized at (111). We shall hereafter call the anisotropy with respect to the surface orientation and that with respect to the direction on a plane the interplanar and intraplanar anisotropies, respectively. It is seen in Fig. 2 that both the interplanar and intraplanar mobility anisotropies are substantially in accord with those of the reciprocal effective mass, and are entirely contrary to the feature of the p-channel result,[1] which is reproduced in the lower half of Fig. 2. Quantitative agreement is not satisfactory, however.

A part of this disagreement is presumed to be due to the fact that the carriers in the z direction are not all in the lowest energy subband. In Fig. 3 we plot the Fermi levels at 300 °K (and 77 °K), the ground states of three different valleys, and the first and second excited states of ⟨100⟩ or ⟨010⟩ valley as functions of the surface orientation in the case of $F_z = 5\times10^5$ V/cm. The calculations were made in the triangular potential approximation. Referring to Table II, we expect that, when adjacent ground states of other valleys are involved (a) m^{-1}(100) is decreased; (b) on (011), $m^{-1} \perp \langle 01\bar{1}\rangle$ is decreased and $m^{-1} \parallel \langle 01\bar{1}\rangle$ is increased; (c) on (hkl) between (111) and (100) in the ⟨01$\bar{1}$⟩ zone, say (311), $m^{-1} \parallel \langle 01\bar{1}\rangle$ is decreased; and (d) on (hkl) between (001) and (011) in the ⟨100⟩ zone, say (013), $m^{-1} \parallel \langle 100\rangle$ is not changed by mixing the states of the ⟨010⟩ valley, but is decreased by the ⟨100⟩ valley. When these effects are taken into account, both the interplanar and intraplanar effective-mass anisotropies approach the experimental mobility anisotropy. In order to obtain numerical values of the reciprocal mass considering the mixing of other valleys and upper subbands, one needs to determine the energy separations more exactly, and then one should make a self-consistent calculation.[5] Preliminary results of Maeda's self-consistent calculation[12] are cited in Table III. Hereafter m^{-1} means a thermally averaged reciprocal effective mass, neglecting the energy dependence of the relaxation time. The anisotropy of the new reciprocal effective mass is in good agreement with the observed mobility anisotropy. This is rather surprising when one considers the energy uncertainty caused by carrier scattering and also by possible anisot-

TABLE III. Preliminary results of a self-consistent calculation of the effective masses in unit of m_e^{-1} of electrons, performed by Maeda (Ref. 11). $F_z = 5\times10^5$ V/cm, $N_A - N_D = 5\times10^{15}$ cm^{-3}, and $N = 3.0\times10^{12}$ cm^{-2}.

	300 °K		77 °K	
	$m_x^{-1} \parallel \langle 100\rangle$	$m_y^{-1} \perp \langle 100\rangle$	$m_x^{-1} \parallel \langle 100\rangle$	$m_y^{-1} \perp \langle 100\rangle$
(001)	4.30	4.30	5.07	5.07
(013)	4.26	3.43	5.04	3.63
(023)	4.20	2.76	4.96	2.34
	$m_x^{-1} \parallel \langle 01\bar{1}\rangle$	$m_y^{-1} \perp \langle 01\bar{1}\rangle$	$m_x^{-1} \parallel \langle 01\bar{1}\rangle$	$m_y^{-1} \perp \langle 01\bar{1}\rangle$
(011)	2.62	4.18	2.00	4.92
(133)	2.75	4.01	2.18	4.67
(111)	3.33	3.33	3.33	3.33
(322)	3.67	3.06	4.19	2.64
(211)	3.88	3.01	4.63	2.57
(311)	4.09	3.20	4.92	3.06
(811)	4.27	3.98	5.06	4.53
(100)	4.30	4.30	5.07	5.07

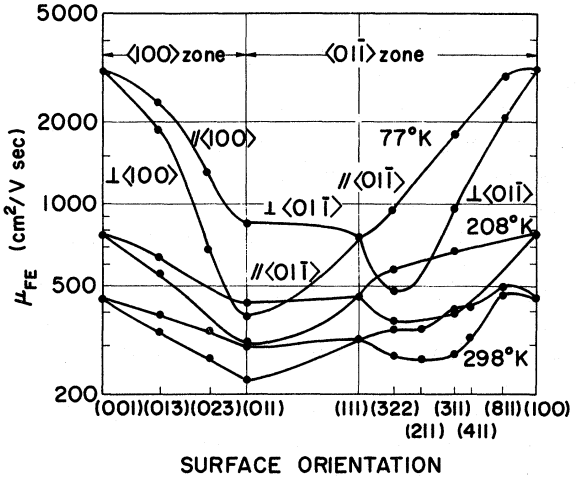

FIG. 4. Field-effect mobilities of electrons observed at 77, 208, and 298 °K as functions of surface orientation and current-flow direction. $F_z = 5\times10^5$ V/cm. The samples are the same as those in Fig. 2. The threshold voltages at 77 and 208 °K (in parentheses) are −1.5 V (−1.1 V), (100); −0.9 V, (811) ∥ ⟨01$\bar{1}$⟩; −1.9 V, (811) ⊥ ⟨01$\bar{1}$⟩; −1.8 V (−2.8 V), (311) ∥ ⟨01$\bar{1}$⟩; −3.2 V (−2.8 V), (311) ⊥ ⟨01$\bar{1}$⟩; −1.6 V (−2.2 V), (322) ∥ ⟨01$\bar{1}$⟩; −1.1 V (−1.5 V), (322) ⊥ ⟨01$\bar{1}$⟩; −3.2 V (−3.7 V), (111); −1.3 V (−2.0 V), (011) ⊥ ⟨01$\bar{1}$⟩; −1.1 V (−1.5 V), (011) ∥ ⟨01$\bar{1}$⟩; −1.3 V, (023) ∥ ⟨100⟩; −1.3 V, (023) ⊥ ⟨100⟩; −1.0 V (−0.5 V), (013) ∥ ⟨100⟩; −1.4 V (−0.5 V), (013) ⊥ ⟨100⟩.

ropy of the relaxation time.

Figure 4 shows the mobility anisotropy at three temperatures: 298, 208, and 77 °K. The change in the anisotropy with temperature is not simple, but in general the interplanar anisotropy is much increased at 77 °K, and the intraplanar anisotropy on the surfaces around the (011) and (111) regions is appreciably increased. The self-consistent calculation[12] has resulted in a comparable intraplanar anisotropy, but in an interplanar anisotropy (see Table III) which is too small for the experimental mobility anisotropy at $V_G' = V_G - V_T = 25$ V and $T = 77$ °K. Although we should not be overly concerned with numerical details, because μ_{FE} at 77 °K strongly depends upon V_G' (see Sec. VI) so that μ_{FE} at $V_G' = 25$ V is only specific, and μ_{FE} deviates from the conductivity mobility (see Sec. III), the large disagreement between theory and experiment requires the investigation of the carrier-scattering mechanism. In what follows we shall approach this problem by studying the dependences of the mobility on the gate field and temperature.

V. DEPENDENCES ON GATE FIELD AND TEMPERATURE

A. Gate-Field Dependence

In Fig. 5 μ_{FE} is plotted as a function of V_G' for typical surface orientations at 298 and 77 °K. A rough feature of the dependence at temperatures in the range 77–320 °K for various orientations may be seen from Figs. 9–13, in which the temperature dependences of μ_{FE} at several values of V_G' are shown.

Near room temperature μ_{FE} is roughly proportional to $(V_G - V_T)^{-1/\gamma}$ with $\gamma = 2.4 \sim 2.8$ over a range of V_G' from 2 to 25 V. It is recognized in the literature that observed values of the electron mobility and the gate-field dependence, except for a weak-field region, are not much scattered among n-channel transistors made on the (100) plane by present technology, although the mobility at the weak gate field is sensitive to the surface-state density.

As shown in Fig. 6, we have made it clear in an independent experiment[13] that the mobility does not depend upon acceptor concentration in the substrate over a wide range, but primarily depends upon $F_z = 4\pi e N_{tot}/\kappa_{Si}$ and not upon N. The notation N_{tot} is the total charge density. The surface-state density in this experiment estimated from the threshold voltage is $1.5 \sim 3.0\times10^{11}/\text{cm}^2$, independent of the substrate resistivity.

The field dependence of μ_{FE} at 77 °K is very anisotropic with regard to the surface orientation, but is similar on the two directions on a plane. Another example is given in Fig. 7 for (811). Two remarkable features in the data are pointed out: One is that the mobility curve on the surfaces that yield relatively higher mobility shows a second peak around $V_G' = 20$V. Fang and Fowler[6] pointed out that the second peak is observed on (100), (001), and (111) at low temperatures below 90 °K, but

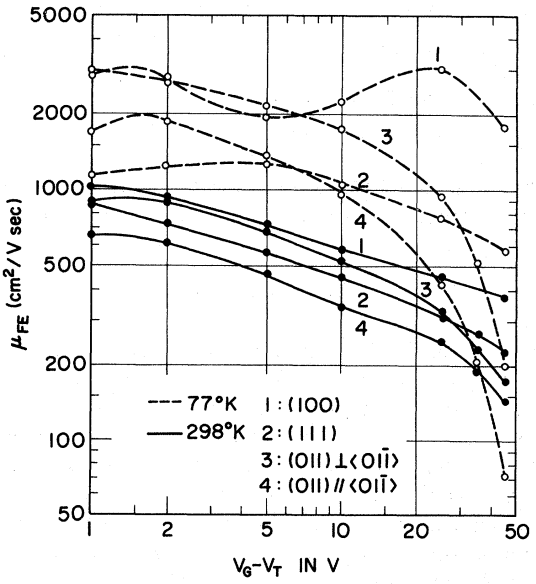

FIG. 5. Gate-field dependence of the field-effect mobility of electrons at 77 and 298 °K for typical surface orientations.

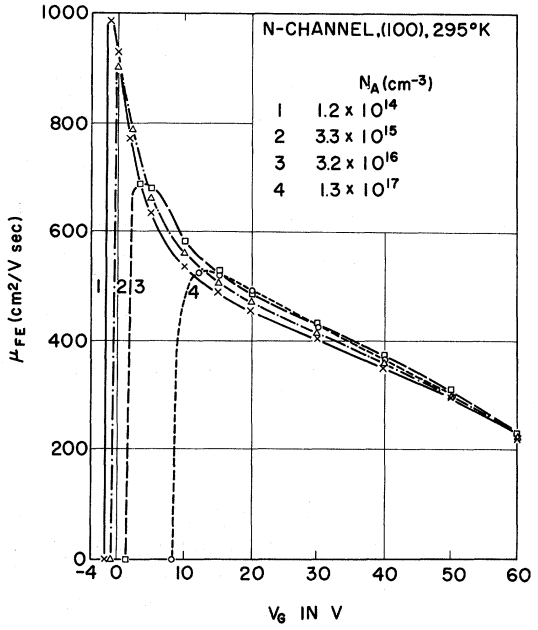

FIG. 6. Plots of the field-effect mobility of electrons on the (100) plane as a function of gate voltage for several substrate acceptor concentrations at 298 °K.

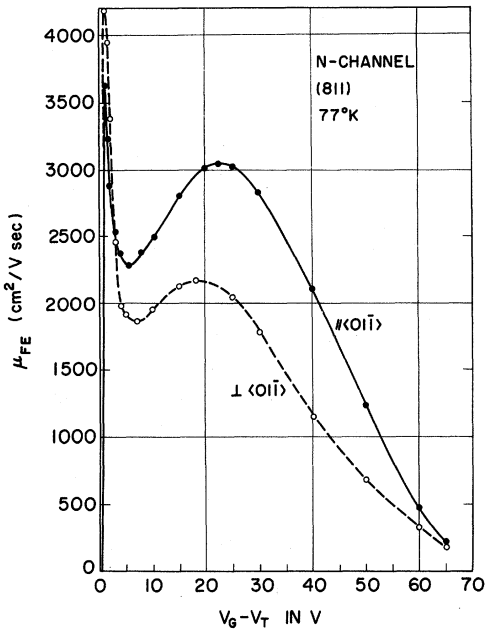

FIG. 7. Field-effect mobility of electrons vs $V_G - V_T$ on the (811) plane with two current-flow directions at 77 °K.

not on (111) with low substrate resistivity. In the present case, besides the data shown in Figs. 5 and 7, the second peak appears on (311) ∥ ⟨01$\bar{1}$⟩ and ⟨013⟩ ⊥ ⟨$\bar{1}$00⟩ and ∥ ⟨100⟩, but not appreciably on (311) ⊥ ⟨01$\bar{1}$⟩ and the remainder. It is thus evident that the second peak is very prominent on the surfaces and the current direction in which the reciprocal effective mass is large. The interesting feature is that μ_{FE} for all orientations become negative at a large V_G' over 50V. The negative field-effect mobility was first reported by Fang and Howard.[14] This is due to a decrease in μ which is faster than F_s^{-1}.

It should be noted that the mobility at 77 °K, in particular at a weak gate field, is more sensitive to the surface-state density than it is at room temperature.[15] In Fig. 8 we reproduce the result of measurement of μ_{FE} at 77 °K for (100) surfaces on the same samples as for Fig. 6. The mobility is again independent of acceptor concentration, but is determined primarily by F_s, excepting only the case of the lowest resistivity. The mobility curve for the sample of the lowest resistivity is somewhat different from the others. That the mobility of the sample is lower around $V_G' = 20$V indicates a contribution of the scattering by bulk impurity whose surface density is now comparable to the density of surface states. Thus, in the samples with lower acceptor concentrations the surface states are main charges scatterers.

Here we compare briefly these results with those of the p channel: Even at room temperature, γ in the range of V_G' from 10 to 25 V has a strong anisotropy (see Figs. 6–8 of Ref. 1 and Figs. 14 and 15 in Sec. VI of this paper). We note that the higher density of surface states on (111) and (011) might play an important role for large γ. Corresponding data on the p channel at 77 °K were described in Figs. 11 and 12 of Ref. 1, and a rough feature on (100) and (011) will be seen in Figs. 14 and 15 in this paper. Like the n-channel result, the inter-

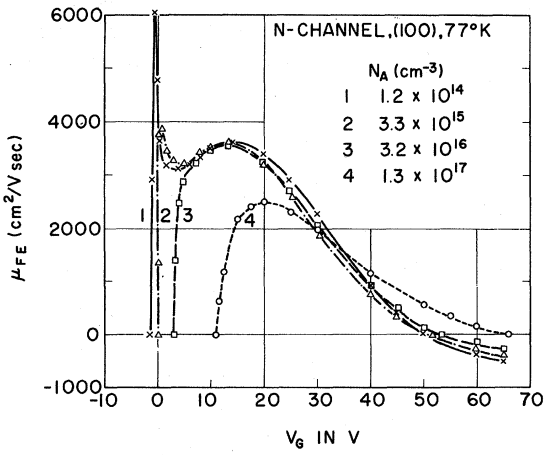

FIG. 8. Plots of the field-effect mobility of electrons on the (100) plane vs gate voltage at 77 °K for several substrate acceptor concentrations. The concentrations shown are the values at room temperature. The samples are the same as for Fig. 6.

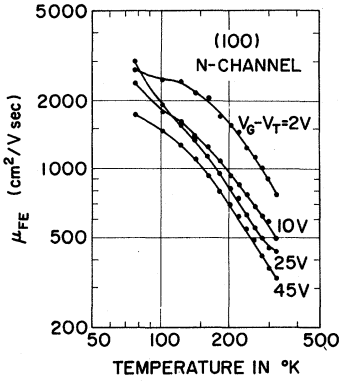

FIG. 9. Temperature dependence of the field-effect mobility of electrons on the (100) plane for several values of $V_G - V_T$.

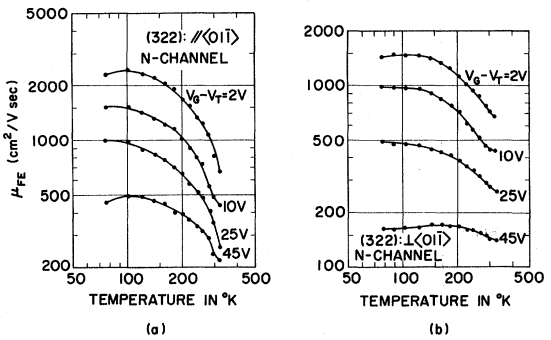

FIG. 11. Temperature dependences of the field-effect mobility of electrons on the (322) plane with two current-flow directions.

planar anisotropy is much increased and the gate-field dependences of μ_{FE} on the two directions on a plane are not much changed.

B. Temperature Dependence

Figures 9–13 show plots of the mobility as a function of temperature in the range 320–77 °K for typical surface orientations at V_G' = 2, 10, 25, and 45 V. The dependence shows inter- and intraplanar anisotropies. The following features may be pointed out. For convenience we write $\mu_{FE} \propto T^{-n}$ with $n(V_G', T)$. (i) On (100), n is scarcely dependent on V_G', and is 1.5 ~ 1.3 above 150 °K (Fig. 9). (ii) On (111), n is 1, nearly independent of V_G' above 200 °K, except for V_G' = 2 V around which n is close to 1.5. (iii) In general, n decreases with increasing V_G' at higher temperatures: The highest value of n is always nearly 1.5 at V_G' = 2 and/or 10 V. At V_G' = 45 V, n is down to 1.0 on (111) and (311) ∥ ⟨01$\bar{1}$⟩, to 0.5 on (311) ⊥ ⟨01$\bar{1}$⟩ and (011) ⊥ ⟨01$\bar{1}$⟩, and even to 0 on (322) ⊥ ⟨01$\bar{1}$⟩ and (011) ∥ ⟨01$\bar{1}$⟩. On (322) ∥ and ⊥ ⟨01$\bar{1}$⟩, and (011) ∥ ⟨01$\bar{1}$⟩, however, n continuously varies with T. (iv) Below 150 °K, n generally decreases with lowering T and sometimes becomes negative, e.g., on (322) ∥ and ⊥ ⟨01$\bar{1}$⟩ at V_G' = 45 V, on (111) at V_G' = 2 V, and on (011) ⊥ and ∥ ⟨01$\bar{1}$⟩ at V_G' = 45 V.

The corresponding data are presented on the p-channel layers on (100) and (011) in Figs. 14 and 15, respectively, for comparison. The result is quite different from the n-channel data on the same surface orientations. The p-channel data on (100) are something like those on the surfaces which show relatively low electron mobility. In contrast, on (011) ∥ ⟨01$\bar{1}$⟩, on which the highest hole mobility is observed, the temperature dependence (n = 1.5 ~ 1.0) is much like that on the (100) which shows the highest electron mobility.

VI. DISCUSSION

The above data on the gate-field and temperature dependences of μ_{FE} are very complicated. The carrier-scattering mechanism should depend upon gate electric field, temperature, surface-state density and its distribution, bulk-impurity concentration, interface perfection, etc. Several scat-

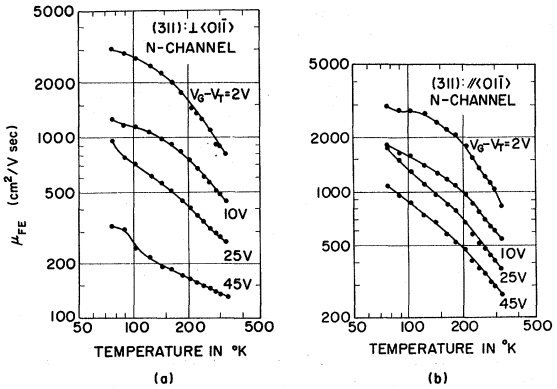

FIG. 10. Temperature dependences of the field-effect mobility of electrons on the (311) plane with two current-flow directions.

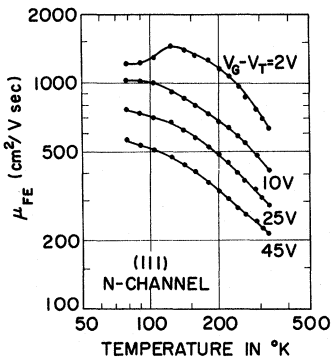

FIG. 12. Temperature dependences of the field-effect mobility of electrons on the (111) plane.

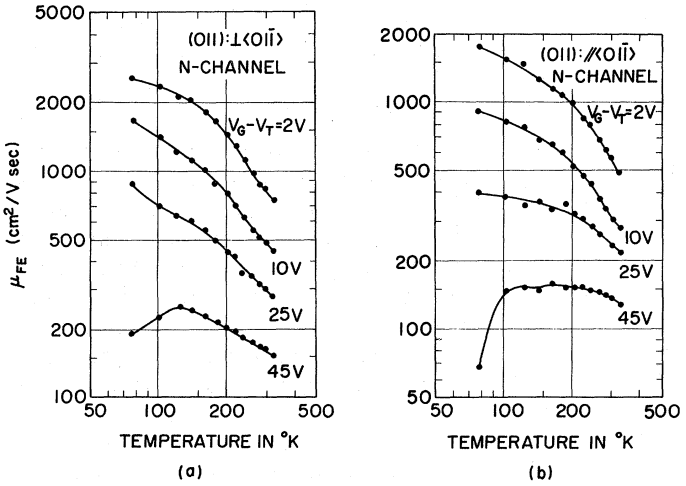

FIG. 13. Temperature dependences of the field-effect mobility of electrons on the (011) plane with two current-flow directions.

tering mechanisms have been studied so far: diffuse scattering, scattering by charged interface impurities, phonons, dislocation, and surface roughness. These theories were critically reviewed recently by Stern.[16] In order to elucidate what mechanism plays a main role for a given experimental condition, one needs to calculate a current in each subband via the given scattering process after finding the number of carriers in each subband. It may be necessary to consider the scattering to upper subbands of the same valley (intersubband scattering) and/or to other valleys (intervalley scattering). No theory that takes account of all of these effects has been available except Siggia and Kwok's general formulation[17] for the case of impurity scattering. Stern and Howard[5] described a practical treatment of screened-Coulomb potential scattering. They computed the mobility of carriers in the lowest subband using a self-consistent potential and compared this with the experimental results of Fang and Fowler[6] at liquid-helium temperature. These theories, however, are not directly applicable to the analysis of the present data covering the high-temperature region. In what follows we restrict ourselves to the investigation of the data rather qualitatively in terms of lattice- and Coulomb-scattering theories. The data on (111) may be most adequate for analysis in terms of any theory in the electric quantum limit, because most of the induced carriers populate in the lowest subband even at room temperature.

First we consider the data near room temperature. The experimental result—$\mu_{FE} \propto (V_G - V_T)^{-1/\gamma}$ with γ close to 3.0 and $\mu_{FE}(111) \propto T^{-1}$—may be interpreted by the two-dimensional lattice-scattering theory. The mobility due to this scattering is expressed as[18,19]

$$\mu_{ij} = \frac{\rho c_i^2 h^3}{\epsilon_1^2 m \| kT} \frac{e}{m_{ij}} \frac{1}{c_n (2 m_z F_z / h^2)^{1/3}}, \quad i, j = 1, 2 \qquad (8)$$

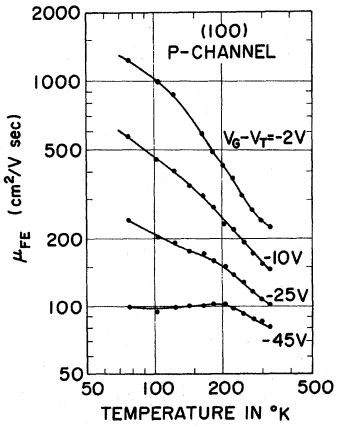

FIG. 14. Temperature dependences of the field-effect mobility of holes on the (100) plane for several values of $|V_G - V_T|$.

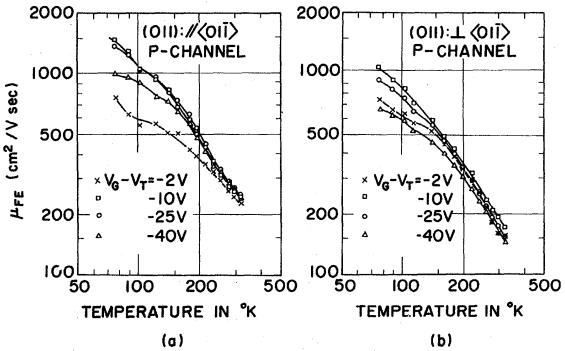

FIG. 15. Temperature dependences of the field-effect mobility of holes on the (011) plane with two current-flow directions.

where ρ is the density of silicon, c_l the sound velocity of the longitudinal mode, ϵ_1 the deformation-potential constant, $m_{\parallel} = (m_x m_y)^{1/2}$ (the density-of-states mass), and $c_1 = 0.418$, $c_2 = 0.291$, ... Kawaji[18] has pointed out that the mobility on (100) at room temperature, measured by Fang and Fowler,[6] obeys the one-third power dependence on N or F_z, but the values of mobility calculated by Eq. (8) using the deformation potential of the bulk are much larger than the observed ones. Ezawa, Kuroda, and Nakamura[20] made a study of scattering by surface waves of the Rayleigh type, but it turned out to be rather ineffective. We note that when the mobility anisotropy is analyzed, possible anisotropy of the deformation potential should be taken into account.

The data at 77 °K cannot be interpreted even qualitatively by existing theories. In the weak gate field, Coulomb scattering by charged scatterers which are most probably charged surface states should play the most important role. The anisotropy of the density and distribution in energy of the surface states is one of the origins of the interplanar anisotropy. The increase in the mobility with N or F_z up to a certain value is due to increased screening and increased carrier energy, as Stern and Howard[5] described in detail. The Coulomb scattering, however, cannot reproduce the observed decrease in the mobility in strong gate fields. The temperature dependence at low temperatures is a very complicated problem, because at low temperatures several scattering mechanisms are competitive.

Concerning the gate-field dependence, the mobility would be decreased with increasing F_z, if the scattering cross section is independent of the carrier velocity, as in classical rigid core scattering, or is increased with increasing carrier velocity. It will be an interesting problem to find a scattering mechanism satisfying this requirement. The scattering by surface roughness[16] is thought to be important for the decrease in the mobility at strong gate fields, but has not been explored enough to compare with experiment. The interface roughness may depend upon the surface orientation, and even upon the crystalline direction on a plane. Even if this is the case, different inter- and intraplanar mobility anisotropies on n- and p-type inversion layers cannot be explained, since the roughness is not different on both type of transistors.

Finally we remark that any theory should explain the mobility anisotropy of both n and p channels which show completely contrary aspects. The effective-mass dependence of the mobility should be $\mu_{ij} \propto m_{ij}^{-p}$, with $p \geq 0$. Other important experimental results remaining unsolved are the second peak in μ_{FE}-vs-F_z curves and the negative field-effect mobility at 77 °K.

VII. CONCLUSIONS

We have studied the mobility anisotropy of electrons in the strongly inverted surface channel, and made it clear that it is principally caused by the effective-mass anisotropy. The mobility anisotropy at room temperature agrees well with the reciprocal-effective-mass anisotropy calculated in a self-consistent scheme. The gate-field and temperature dependences near room temperature, in particular on (111), can be explained by the longitudinal-phonon-scattering theory, but the absolute value of the observed mobility cannot be reproduced unless a larger deformation potential than that in the bulk is assumed. It will be worthwhile to take account of the anisotropy of the deformation potential.

At 77 °K the mobility anisotropy is more pronounced. The increased intraplanar anisotropy is partly interpreted again in terms of the increased effective-mass anisotropy. On the other hand, the interplanar mobility anisotropy is too large to be accounted for in terms of the effective mass. This points to the anisotropy of the relaxation time. None of the known scattering theories, however, is successful in elucidating this large mobility anisotropy, even if the change in the effective mass with gate field and temperature is fully included. We have had several important experimental results which remain unexplained. Of particular interest are (i) the above-mentioned large interplanar mobility anisotropy at 77 °K, (ii) the second peak in the mobility profile against the gate field at 77 °K, which appears on the limited surface orientations showing relatively higher mobility, (iii) the negative field-effect mobility at a strong gate field and at low temperature, and (iv) the complicated temperature dependence of the mobility on some surface orientations at a strong gate field and at low temperatures.

The gate-field and temperature dependences of the hole mobility have some different aspects from those of the electron mobility. This may be primarily due to the different dependence of the effective mass on the surface orientation.

ACKNOWLEDGMENTS

The authors gratefully acknowledge valuable discussions with H. Maeda and prepublication access to results of his theoretical studies, as well as his critical reading of the manuscript. It is a pleasure to thank H. Ohnuma for help in the sample preparation, and K. Ohuchi, T. Shimoma, and K. Shibata for temporary help in making the measurements.

[1] T. Sato, Y. Takeishi, and H. Hara, Japan. J. Appl. Phys. 8, 588 (1969).

[2] H. Maeda (unpublished).

[3] H. Miyazawa, K. Suzuki, and H. Maeda, Phys. Rev.

131, 2442 (1963).
[4]D. Colman, R. T. Bate, and J. P. Mize, J. Appl. Phys. 39, 1923 (1968).
[5]F. Stern and W. E. Howard, Phys. Rev. 163, 816 (1967).
[6]F. F. Fang and A. B. Fowler, Phys. Rev. 169, 619 (1968).
[7]N. St. J. Murphy, F. Berz, and I. Flinn, Solid State Electron. 12, 775 (1969).
[8]A. Ohwada, H. Maeda, and K. Tanaka, Japan. J. Appl. Phys. 8, 629 (1969).
[9]J. R. Schrieffer, in *Semiconductor Surface Physics*, edited by R. H. Kingston (Pennsylvania U. P., Philadelphia, 1956), p. 55.
[10]C. J. Rauch, J. J. Stickler, H. J. Zeiger, and G. S. Heller [Phys. Rev. Letters 4, 64 (1960)] reported the values of $m_t = (0.192 \pm 0.001)m_e$ and $m_l = (0.90 \pm 0.02)m_e$, determined by cyclotron resonance using a wavelength of 2 mm, but no explanation was given of the discrepancy between these values of m_l and $m_l = (0.98 \pm 0.04)m_e$ [G. Dresselhaus, A. F. Kip, and C. Kittel, Phys. Rev. 98, 368 (1955)].
[11]H. Sakaki, T. Hoh, and T. Sugano, IEEE Trans. Electron. Devices ED-17, 892 (1970).
[12]H. Maeda (unpublished).
[13]The sample preparation in this experiment is somewhat different from the preparation for the samples used in the main study of this paper.
[14]F. F. Fang and W. E. Howard, Phys. Rev. Letters 16, 797 (1966).
[15]T. Sugano, H. Sakaki, and K. Hoh, J. Japan. Soc. Appl. Phys. Suppl. 39, 192 (1970).
[16]F. Stern, in Proceedings of the Tenth International Conference on the Physics of Semiconductors, Cambridge, Mass., 1970, p. 451 (unpublished).
[17]E. D. Siggia and P. C. Kwok, Phys. Rev. B 2, 1024 (1970).
[18]S. Kawaji, J. Phys. Soc. Japan 27, 906 (1969).
[19]c_n is the coupling constant in the nth subband and is given, in the triangular potential approximation, by

$$c_n = \frac{1}{2\pi}\int_{-\infty}^{\infty}\left(\frac{|\int_{-\gamma_n}^{\infty}\phi^2(\gamma)e^{-il\gamma}d\gamma|^2}{|\int_{-\gamma_n}^{\infty}\phi^2(\gamma)d\gamma|^2}\right)dl,$$

where ϕ_n is the Airy function and γ_n is the nth root of the Airy function.
[20]H. Ezawa, T. Kuroda, and K. Nakamura, Surface Sci. 24, 654 (1971).

PHYSICAL REVIEW B VOLUME 4, NUMBER 6 15 SEPTEMBER 1971

Exact Solutions of the Kinetic Equations Governing Thermally Stimulated Luminescence and Conductivity

Paul Kelly and M. J. Laubitz
Division of Physics, National Research Council, Ottawa, Canada

and

Peter Bräunlich
Bendix Research Laboratories, Southfield, Michigan 48075
(Received 9 April 1971)

Past analyses of the kinetic equations governing thermally stimulated luminescence and conductivity have invariably involved certain approximations; however, the validity of these approximations has never been explicitly determined. In this paper we give a procedure for determining the conditions under which the approximations are valid, and show that for a model involving a single trap depth in the presence of other deep traps, and a single type of recombination center, the validity depends critically on N, the number of active traps. For $N < 10^{15}$ cm^{-3} the conventional approximations are inadequate, and the kinetic equations must be analyzed exactly through numerical solutions. Although no such solutions have been reported in the literature, we show that they are not only possible, but are in fact readily obtained for certain parametric ranges. Examination of these exact solutions for small N reveals new features; in particular, the dependence of the processes on the density of deep traps, or on initial filling ratios of the active traps, is markedly different from the dependence at large N, where the approximations do hold. This invalidates, for these low densities, many approaches to the analysis of the phenomena which have been recommended on the basis of these approximations. The procedures developed here have been applied to one specific model. However, they can be readily generalized to the solutions of the equations for more complex and realistic models of solids.

I. INTRODUCTION

Thermally stimulated luminescence (TSL) and thermally stimulated conductivity (TSC) are phenomena frequently investigated, mainly because of experimental simplicity and deceptive ease of analysis purportedly yielding useful information on the trapping parameters of solids. An early explana-